Karlsruher Institut für Technologie
Institut für Baustatik

Enhanced studies on a composite time integration scheme in linear and non-linear dynamics

S. Klarmann, W. Wagner

Mitteilung 2(2014)

BAUSTATIK

Karlsruher Institut für Technologie
Institut für Baustatik

Enhanced studies on a composite time integration scheme in linear and non-linear dynamics

S. Klarmann, W. Wagner

Mitteilung 2(2014)

Prof. Dr.–Ing. W. Wagner
Institut für Baustatik
Karlsruher Institut für Technologie
Kaiserstr. 12
76131 Karlsruhe

Telefon: +49 721 608 42280
Telefax: +49 721 608 46015
E–mail: info@ibs.kit.edu
Internet: http://www.ibs.kit.edu

Enhanced studies on a composite time integration scheme in linear and non-linear dynamics

S. Klarmann

Fachgebiet Festkörpermechanik
Technische Universität Darmstadt
Petersenstr. 13
64287 Darmstadt
Germany

W. Wagner

Institut für Baustatik
Karlsruher Institut für Technologie
Kaiserstraße 12
76131 Karlsruhe
Germany

Contents

Summary In [Bathe and Baig(2005)], [Bathe(2007)], [Bathe and Noh(2012)] Bathe et.al. have proposed a composite implicit time integration scheme for non-linear dynamic problems. This paper is aimed at the further investigation of the scheme's behaviour for use in case of linear and non-linear problems. Therefore, the examination of the amplification matrix of the scheme will be extended in order to get in addition the properties for linear calculations. Besides, it will be demonstrated that the integration scheme also has an impact on some of these properties when used for non-linear calculations. In conclusion, a recommendation for the only selectable parameter of the scheme will be given for application in case of geometrically non-linear calculations.

1 Introduction

In the past, a lot of research effort has been carried out in solving differential equations of motion in time. In general, the desired property of an associated integration scheme within a finite element application is unconditional stability of the procedure in order to get an efficient method by using large time steps. In case of linear calculations, there are many schemes,

which exhibit this property. Applying these schemes to non-linear problems, unstable and non-reliable results may be produced.
However, there are schemes, which are able to produce reliable results even in the non-linear range. *Kuhl and Crisfield* [Kuhl and Crisfield(1999)] have categorized the existing schemes in three groups. The first is based on the enforced conservation of energy. Here Lagrangian multipliers are used to produce stable solutions. In another group the idea of algorithmic conservation of energy is introduced, resulting in modifications on element level, which may lead to non-symmetric matrices. For both groups additional operations are necessary before the corresponding schemes can be applied successfully.
In the third group numerical dissipation is used in order to achieve stable calculations of non-linear problems. Here, one of the main advantages is the general applicability of these schemes without the need of further modifications. Hence, no modifications on element level are necessary and existing element formulations can be used directly within these schemes. The scheme discussed within the scope of this paper belongs to this third group. Bathe and co-workers proposed this scheme for structural dynamic problems and presented research results on the behaviour of the scheme ([Bathe and Baig(2005)], [Bathe(2007)], [Bathe and Noh(2012)]). Typically, the authors have used the analysis of the amplification matrix, see [Hoff and Pahl(1988)], [Hoff and Pahl(1988-2)], [Hughes(2000)]. In the upcoming study, we will pick up these evaluations, describe the main essentials and extend them with several further aspects.

2 Theory

As a start, a short summary of the applied scheme is given. According to [Bathe and Baig(2005)] the scheme subdivides the chosen time step into two substeps. If the time step size is Δt then the first substep is equal to $\gamma \cdot \Delta t$ and the second substep is equal to $(1-\gamma) \cdot \Delta t$. For the first substep the well known trapezoidal rule will be used. Afterwards, a three-point Euler backward method will be applied in the second substep.

2.1 Trapezoidal rule

As already mentioned, the scheme uses the trapezoidal rule [Newmark(1959)] for the calculation of the first substep. Therefore, a constant average acceleration is assumed within this time interval. After a simple integration with respect to the integration limits of the composite scheme one ends up with the following equations for the first substep

$$ {}^{t+\gamma\Delta t}\mathbf{U} = {}^{t}\mathbf{U} + {}^{t}\dot{\mathbf{U}} \cdot \gamma \cdot \Delta t + \frac{{}^{t}\ddot{\mathbf{U}} + {}^{t+\gamma\Delta t}\ddot{\mathbf{U}}}{4} \cdot (\gamma \cdot \Delta t)^2 \tag{1} $$

$$ {}^{t+\gamma\Delta t}\dot{\mathbf{U}} = {}^{t}\dot{\mathbf{U}} + \frac{{}^{t}\ddot{\mathbf{U}} + {}^{t+\gamma\Delta t}\ddot{\mathbf{U}}}{2} \cdot \gamma \cdot \Delta t \tag{2} $$

2.2 Euler backward

Following the first substep, the second step can now be calculated by use of the Euler backward scheme. Here, one obtains the equations

$$ {}^{t+\Delta t}\dot{\mathbf{U}} = a_1 \cdot {}^{t}\mathbf{U} + a_2 \cdot {}^{t+\gamma\Delta t}\mathbf{U} + a_3 \cdot {}^{t+\Delta t}\mathbf{U} \tag{3} $$

$$ {}^{t+\Delta t}\ddot{\mathbf{U}} = a_1 \cdot {}^{t}\dot{\mathbf{U}} + a_2 \cdot {}^{t+\gamma\Delta t}\dot{\mathbf{U}} + a_3 \cdot {}^{t+\Delta t}\dot{\mathbf{U}} \tag{4} $$

with parameters a_1 to a_3

$$ a_1 = \frac{1-\gamma}{\gamma \Delta t} \tag{5} $$

$$ a_2 = \frac{-1}{(1-\gamma)\cdot\gamma\cdot\Delta t} \tag{6} $$

$$ a_3 = \frac{2-\gamma}{(1-\gamma)\cdot\Delta t} \tag{7} $$

2.3 Implementation

The implementation of the scheme has been conducted straight forward, see [Bathe and Baig(2005)], [Bathe(2007)], [Bathe and Noh(2012)], and is summarized below. First, one has to solve the equations of motion

$$ {}^{\delta}\mathbf{R} = \mathbf{M}\ {}^{\delta}\ddot{\mathbf{U}} + \mathbf{C}\ {}^{\delta}\dot{\mathbf{U}} + \mathbf{F}_{int}\left({}^{\delta}\mathbf{U}\right) - {}^{\delta}\mathbf{F}_{ext} = \mathbf{0} \tag{8} $$

at the specific time $\delta = t+\gamma\Delta t$ and $\delta = t+\Delta t$, by means of the mass matrix $\mathbf{M}$, the damping matrix $\mathbf{C}$, the vector of internal forces ${}^{\delta}\mathbf{F}_{int}$ and the vector of external loads ${}^{\delta}\mathbf{F}_{ext}$.
In order to solve the given system of equations the well-known Newton-Raphson scheme is applied after expressing ${}^{\delta}\ddot{\mathbf{U}}$ and ${}^{\delta}\dot{\mathbf{U}}$ in terms of ${}^{\delta}\mathbf{U}$. It follows the following algorithm:

1. Set $\delta = t + \gamma\Delta t$
2. Assume ${}^{\delta}\mathbf{U} = {}^{t}\mathbf{U}$ and set up ${}^{\delta}\ddot{\mathbf{U}}$, ${}^{\delta}\dot{\mathbf{U}}$ with sec. 2.1
3. Calculate ${}^{\delta}\mathbf{R}$ and ${}^{\delta}\mathbf{K}_{eff}$
4. Solve ${}^{\delta}\mathbf{K}_{eff}\Delta\mathbf{U} = -{}^{\delta}\mathbf{R}$
5. Update ${}^{\delta}\mathbf{U}$ and ${}^{\delta}\ddot{\mathbf{U}}$, ${}^{\delta}\dot{\mathbf{U}}$ with sec. 2.1
6. Check convergence
   no: goto 3
   yes: continue
7. Set $\delta = t + \Delta t$
8. Assume ${}^{\delta}\mathbf{U} = {}^{t+\gamma\Delta t}\mathbf{U}$ and set up ${}^{\delta}\ddot{\mathbf{U}}$, ${}^{\delta}\dot{\mathbf{U}}$ with sec. 2.2
9. Calculate ${}^{\delta}\mathbf{R}$ and ${}^{\delta}\mathbf{K}_{eff}$
10. Solve ${}^{\delta}\mathbf{K}_{eff}\Delta\mathbf{U} = -{}^{\delta}\mathbf{R}$
11. Update ${}^{\delta}\mathbf{U}$ and ${}^{\delta}\ddot{\mathbf{U}}$, ${}^{\delta}\dot{\mathbf{U}}$ with sec. 2.2
12. Check convergence
    no: goto 9
    yes: continue and set $t = \delta$

The vector ${}^{\delta}\mathbf{R}$ is presented in Eq. 8, where ${}^{\delta}\mathbf{K}_{eff}$ is calculated from ${}^{\delta}\mathbf{K}_{eff} = \partial {}^{\delta}\mathbf{R}/\partial {}^{\delta}\mathbf{U}$. Further details can be found in [Bathe and Baig(2005)].

3 Analytical study

After this short insight into the main features of the scheme, an analytical analysis of its application for linear problems is performed in the upcoming part. As already discussed in [Bathe and Baig(2005)], [Bathe(2007)] and [Bathe and Noh(2012)] it can be stated that the scheme is second order accurate, unconditionally stable and possesses a desirable amount of numerical damping. This analysis shall now be extended by focussing on the only free parameter γ. In order to keep this analysis as simple as possible, the amplification matrix $\mathbf{A}$ is generated without physical damping and load operators. It follows

$$\begin{bmatrix} {}^{t+\Delta t}U \\ {}^{t+\Delta t}\dot{U} \\ {}^{t+\Delta t}\ddot{U} \end{bmatrix} = \mathbf{A} \begin{bmatrix} {}^{t}U \\ {}^{t}\dot{U} \\ {}^{t}\ddot{U} \end{bmatrix} \tag{9}$$

leading to the following form of the amplification matrix

$$\mathbf{A} = \frac{1}{\alpha} \left[\begin{array}{c|c|c} \beta_1 & \beta_2 & 2-\gamma^2 \\ -\beta_3\Omega^2 & \beta_4 & \gamma^2\Omega^2 - \gamma\Omega - 2\gamma + 4 \\ -\beta_1\Omega^2 & -\beta_2\Omega^2 & \Omega^2(\gamma^2-2) \end{array}\right] \tag{10}$$

The parameters used are

$$\begin{aligned} \alpha &= (\gamma^2\Omega^2 - 2\gamma\Omega^2 + \Omega^2 + \gamma^2 - 4\gamma + 4)(\gamma^2\Omega^2 + 4) \\ \beta_1 &= \gamma^4\Omega^2 - 4\gamma^3\Omega^2 + 5\gamma^2\Omega^2 - 2\Omega^2 + 4\gamma^2 - 16\gamma + 16 \\ \beta_2 &= \gamma^4\Omega^2 - 3\gamma^3\Omega^2 + 4\gamma^2\Omega^2 - 2\gamma\Omega^2 + 4\gamma^2 - 16\gamma + 16 \\ \beta_3 &= \gamma^4\Omega^2 - 3\gamma^3\Omega^2 + 3\gamma^2\Omega^2 - \gamma\Omega^2 + 4\gamma^2 - 14\gamma + 12 \\ \beta_4 &= \gamma^4\Omega^2 - 4\gamma^3\Omega^2 + 6\gamma^2\Omega^2 - 4\Omega^2 + 4\gamma^2 - 16\gamma + 16 \end{aligned} \tag{11}$$

For convenience, it was chosen $\Omega = \omega \cdot \Delta t$. The eigenvalues of the amplification matrix $\mathbf{A}$ are given by

$$\lambda_1 = \frac{2\gamma + (i\gamma^2 - 2i\gamma + 2i)\Omega - 4}{(\gamma - \gamma^2)\Omega^2 + (i\gamma^2 - 2i)\Omega + 2\gamma - 4} \tag{12}$$

$$\lambda_2 = \frac{2i\gamma + (\gamma^2 - 2\gamma + 2)\Omega - 4i}{(i\gamma - i\gamma^2)\Omega^2 + (\gamma^2 - 2)\Omega + 2i\gamma - 4i} \tag{13}$$

The third eigenvalue is zero. Now we can present and discuss the properties of the scheme. A good overview of the necessary equations can be found in e.g. [Hoff and Pahl(1988)]. Fig. 1 shows the spectral radius $\rho(\mathbf{A})$ by use of a logarithmic scale. It can be seen that a value of ($\rho = 1$ occurs in the low frequency range, whereas it tends to $\rho = 0$ for higher frequencies. Obviously, the scheme filters these frequencies rather than damping them out. Another point to be mentioned is the unconditional stability of the scheme for all values of $\gamma \in (0, 1)$.
Figs. 2 to 4 illustrate the properties of the spectral radius, the period elongation and the amplitude decay in the low frequency range. To improve the visualization different orientations of the axes $\frac{\Delta t}{T}$ and γ have been chosen. It is interesting to note that the plotted functions show

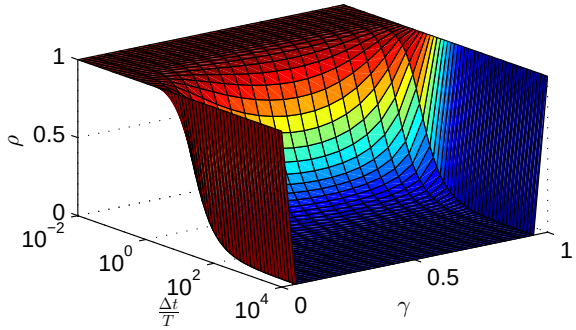

Figure 1: Spectral radius - overall range

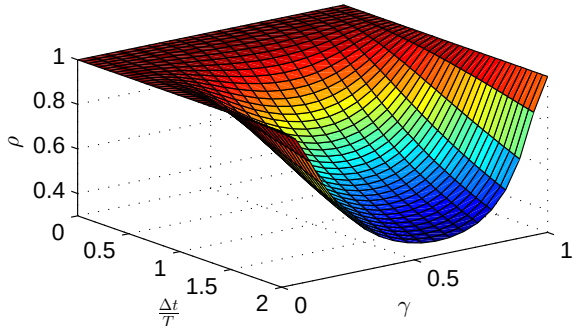

Figure 2: Spectral radius - low frequency range

their respective extreme values for the same value of γ. To determine this value, we assume a linear calculation with $\Delta t = \text{const.}$ which also results in a constant value of ω. Subsequently, a functional analysis only depending on the free parameter γ can be performed, leading to

$$\gamma = 2 - \sqrt{2}\,. \tag{14}$$

as a minimum. This value is already known but for another kind of reason. According to [Bathe and Noh(2012)] the tangent stiffness matrix has to be calculated only once for $\gamma = 2 - \sqrt{2}$. Here we have shown that this value results in a respective minimum for the spectral radius and the period elongation, as well as a maximum for the energy dissipation regarding the γ-direction.
In order to conclude this section, a comparison of the discussed scheme (Bathe, γ) with the generalized-α-method (GENA, ρ_∞) [Chung and Hulbert(1993)] and the HHT-α-method [Hilber,Hughes,Taylor(1977)] (HHT, ρ_∞), is presented in addition to [Bathe and Noh(2012)].

Fig. 5 shows a comparison of the spectral radius which starts to drop around the same value $\Delta t/T$ for the depicted schemes. As it can be seen, the main difference between the schemes occurs in the high frequency range. While the spectral radius of the generalized-α- and HHT-α-method tends against a specific value ρ_∞, the one of the Bathe scheme drops to zero.
From Fig. 6 one can deduce that the period elongation per time step is lower than the one of the generalized-α- or HHT-α-method. However, regarding the numerical effort, we have to keep in mind that the Bathe scheme needs two solution processes, one for $t + \gamma\Delta t$ and one for $t + \Delta t$, to complete one time step.

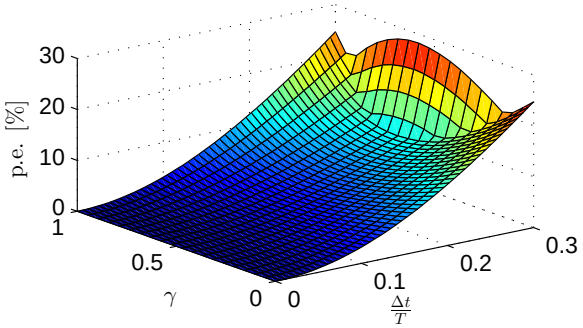

Figure 3: Period elongation - low frequency range

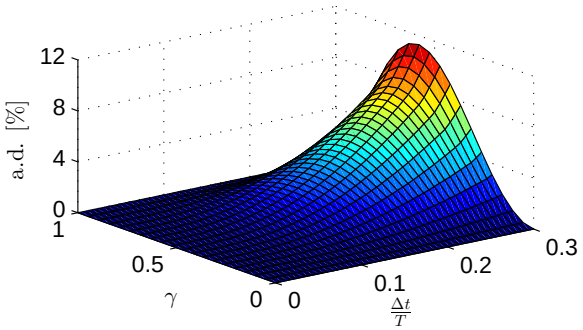

Figure 4: Amplitude decay - low frequency range

Fig. 7 shows the amplitude decay of the scheme. Analogous to the period elongation, the amplitude decay of the schemes starts around the same value of $\Delta t/T$ and a similar shape of the curves occurs.

4 Numerical examples-results, aspects and modifications

In section 3 we have presented the properties of the scheme with respect to the parameter γ. The results can be easily verified by applying the scheme to linear problems, as it will be demonstrated in the upcoming section. In contrast, examples based on non-linear calculations will lead to a deviant behaviour of the scheme. Hence, it can be shown that the scheme is no longer stable for arbitrary values of γ and a different damping behaviour in the non-linear range, depending at least on the model, occurs. A further noticeable effect has been identified when accelerations for geometrically non-linear calculations are investigated. In this case, an overrated first substep can be observed which is corrected by the second substep leading to incorrect values for both of them. The influence of this effect obviously depends on the choice of γ and Δt and will be discussed by some examples. Furthermore, a recommendation for an 'optimal' choice of γ will be given.
In the following diagrams we use the notation *Bathe*,γ to describe the different behaviour of the scheme. Thus *Bathe*,0.5 means that we choose the discussed algorithm by means of a value of $\gamma = 0.5$.

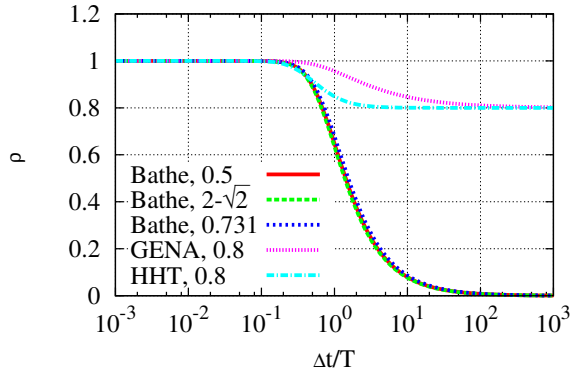

Figure 5: Spectral radius for different time integration schemes

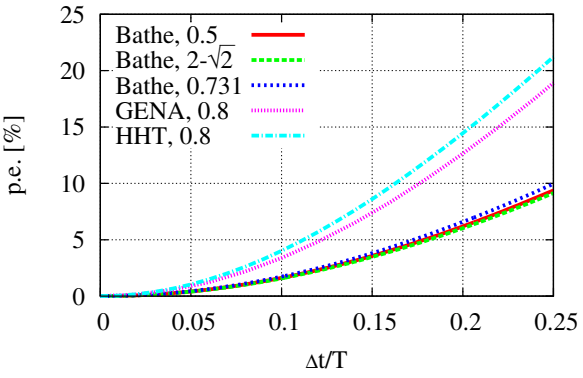

Figure 6: Period elongation for different time integration schemes

4.1 Stiff pendulum - truss: Energy dissipation

As introductory example the common problem of a stiff pendulum is discussed, see e.g. [Kuhl and Crisfield(1999)]. At first, the original model according to Fig. 8 is investigated. The parameters are $l = 3.0443\,m$, $m = 10\,kg$, $EA = 10^{10}\,N$, $\dot{u} = 7.72\,m/s$, and $\ddot{u} = 19.8\,m/s^2$. As already mentioned before the proposed scheme does yield reliable results for this kind of problem and one can calculate the energy as a function the parameter γ, as shown in Fig. 9. Regarding the values $\gamma = 2 - \sqrt{2}$ and the lower ones, it can be noticed that the energy dissipation decreases with decreasing values of γ. This behaviour is in accordance to the analysis in section 3, except that the energy increases for the value $\gamma = 0.3$ and the scheme gets unstable. For increasing values of γ the energy dissipation increases. This fact is in contrast to the analysis of section 3. Thus, the scheme changes its properties, regarding numerical damping and stability, when applied to a non-linear calculation. Another point to mention is, that there should exist one value of γ for which the scheme is energy conserving. As this value is apparently dependent on the chosen model, its influence will not further be investigated at this point but in the upcoming part. These results are similar to the one of [Matias Silva and Mendes Bezerra(2008)].

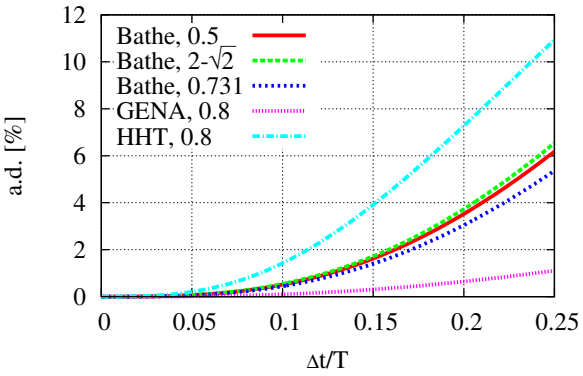

Figure 7: Amplitude decay for different time integration schemes

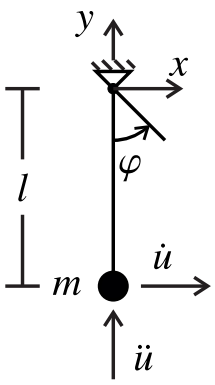

Figure 8: Original stiff pendulum, truss model

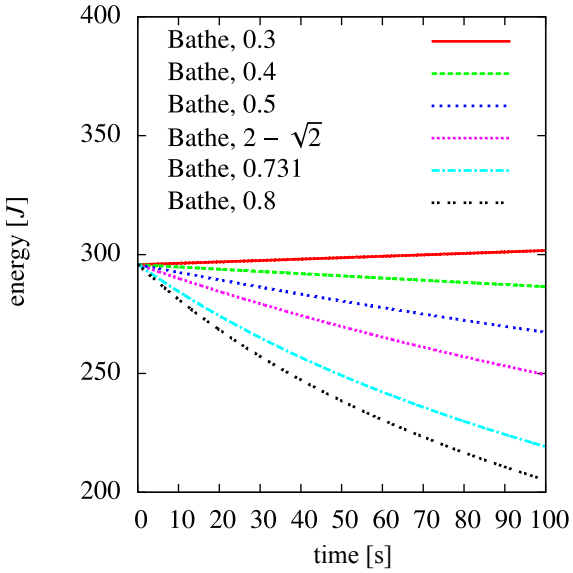

Figure 9: Energy vs. time for $\Delta t = 0.1$ s

4.2 Stiff pendulum - Timoshenko beam: influence of substeps

It has been demonstrated that the properties of the scheme can change in case of non-linear calculations. Hence, several modifications to the model are introduced yielding further interesting effects. In a second example the truss element is thus replaced by a finite rotation Timoshenko beam element based on a Green-Lagrangian strain tensor, similar to [Wagner(1990)].

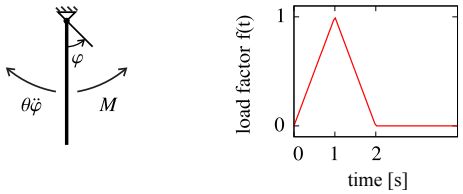

Figure 10: Stiff pendulum, beam model and loading function f(t)

Fig. 10 shows the modified model of the stiff pendulum and a loading function $f(t)$, where M is the applied momentum and θ the mass moment of inertia. The chosen model parameters are $EA = 10^{12}\,N$, $EI = 10^{11}\,Nm^2$, $\kappa GA = 4.167\,10^{11}\,N$ and $\rho = 0.3\,kg/m^3$. As reference the analytical solution of a rigid body rotation is used. To get converged results, 20 two-node elements are introduced and a consistent mass matrix formulation is applied. The rotation starts according to the loading function $f(t)$ with $M = M_0 \cdot f(t)$ and $M_0 = 600\,Nm$. In the following, the total energy of the system shall be observed. For that purpose at time step of $\Delta t = 0.1\,s$ is chosen to provoke a higher influence of the numerical damping.

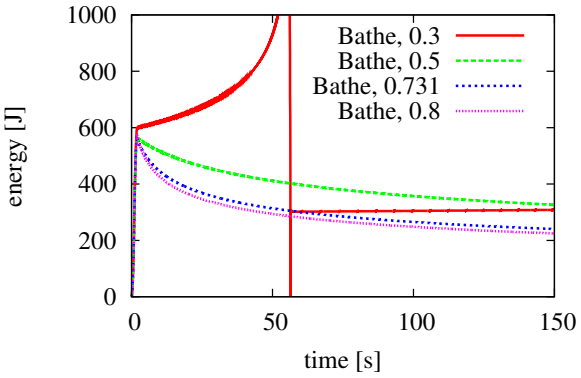

Figure 11: Energy dissipation - $\Delta t = 0.1$ s

The associated energy progress with respect to time is depicted in Fig. 11. The general behaviour is comparable to the one of the previous diagram. For $\gamma = 0.3$ the scheme gets unstable, while the other values of γ result in stable solutions. Again the energy dissipation is increasing with increasing γ. A reduction of Δt to $0.01\,s$ leads to the diagram in Fig. 12 with a further decrease of energy dissipation. The scheme approaches an energy conserving behaviour. The sequence of the curves for the different values of γ is the same as before. Having a closer look at the results for $\gamma = 0.3$ a slightly energy growth can still be noticed.
As a next step, the behaviour in φ-direction at the center of the rotation for a value of $\Delta t = 0.01\,s$ is determined.

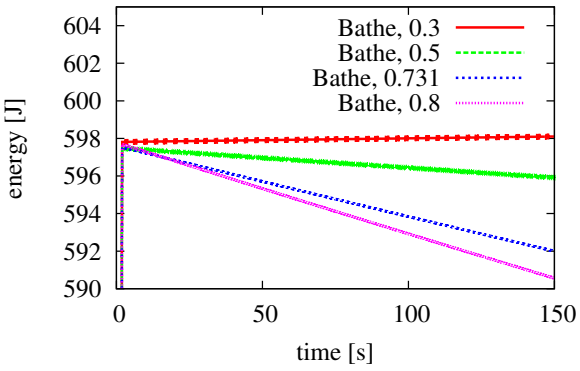

Figure 12: Energy dissipation - $\Delta t = 0.01$ s

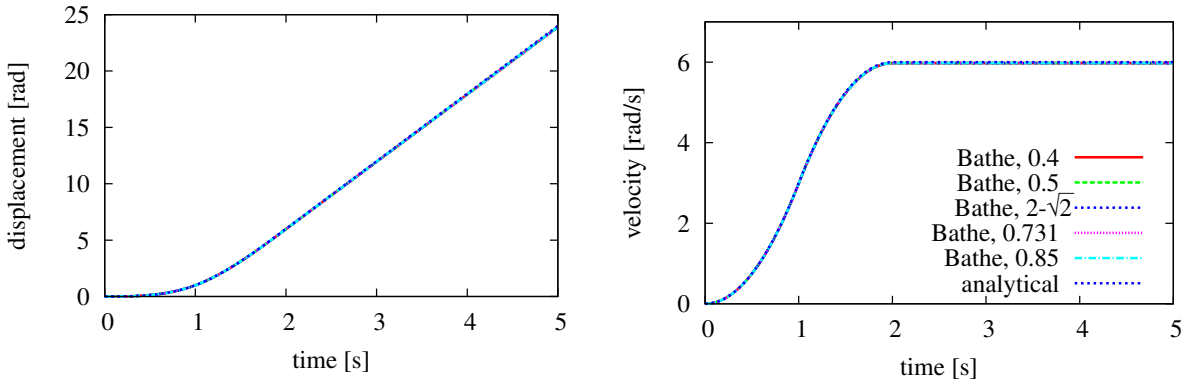

Figure 13: Angular displacement and velocity vs. time - $\Delta t = 0.01$

Fig. 13 shows the calculated angular displacements and velocities of the scheme for different values of γ in comparison to the analytical solution based on a rigid body rotation. Good agreement with the reference solution for all chosen values of γ can be observed.
The results of the angular accelerations $\ddot{\varphi}$ are of higher significance though. They are presented separately for each value of γ in the upcoming figures.
Fig. 14 shows the solution of the scheme for the angular accelerations in case of $\gamma = 0.4$. In this diagram results are depicted for the value of the first and second substep, as well as the analytical solution. It is worth noting that the scheme remains stable by means of these settings, even though the results of the accelerations oscillate around the analytical solution. Regarding the first substep the scheme yields results which are higher than those of the analytical solution, whereas the second substep produces results less than the analytical solution. Hence, both approaches are insufficient yielding too large deviations. It should be noted that the first substep can be considered as an intermediate step having no further relevance, whereas the results obtained after the second substep should describe the physical behaviour correctly.
Fig. 15 shows the results for $\gamma = 0.5$. It can be clearly seen that the effect of oscillating accelerations has decreased with the increasing value of γ.
Next, results for a further increase of γ are presented, for instance Fig. 16 shows results for $\gamma = 0.85$. Concerning this problem, two effects can be observed. The first one is the fact that the gap between the first and second substep decreases even further. The second effect is that in contrast to the previous figures, the order of substep curves has changed. In this

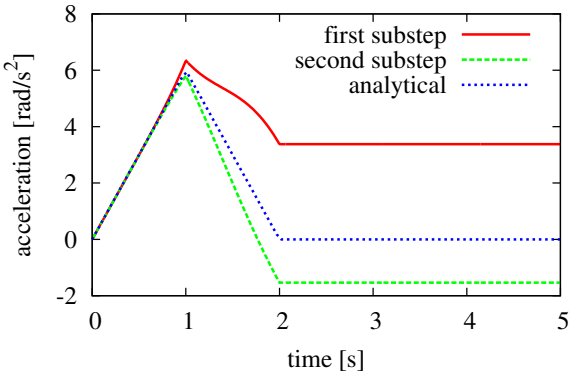

Figure 14: Angular accelerations for $\gamma = 0.4$ vs. time - $\Delta t = 0.01$ s

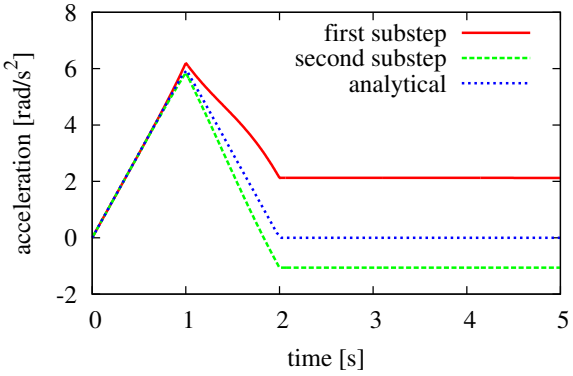

Figure 15: Angular accelerations for $\gamma = 0.5$ vs. time - $\Delta t = 0.01$ s

case, results concerning the first substep are below and results concerning the second substep are above the reference values. Obviously, there must be an 'optimal' value of γ for which the scheme provides an accurate solution for the accelerations.
By means of an iterative development, an associated 'optimal' value of $\gamma = 0.731$ is identified. The corresponding diagram is illustrated in Fig. 17 where the results of the scheme matches the analytical solution.
Finally, the time step size Δt is reduced to $0.001\,s$ and the calculated accelerations of the scheme for $\gamma = 0.5$ and $\gamma = 0.731$ are compared to one another.
Accordingly, Fig. 18 shows the results for $\gamma = 0.5$. It can be seen that the effect is reduced but still present. This should not be surprising as with a reduction of Δt the solution is assumed to converge against the analytical one. The choice of $\gamma = 0.731$ leads for $\Delta t = 0.001\,s$ again to accurate results, see Fig. 17.
Hence, in conclusion there are two options to improve the accuracy of the calculated accelerations. One option is to reduce the time step size Δt and the other one is to choose an 'optimal' value of γ, here $\gamma = 0.731$.
In addition, these results demonstrate that the scheme produces smooth but eventually incorrect solutions regarding only the first or second substep. If the first substep is seen as an intermediate technical substep with no physical meaning, then the associated results can be omitted. Tough starting with a wrong first substep leads to a wrong calculated second substep, and thus overall solution is not correct. Consequently, a adequate choice of γ is necessary to get appropriate results.

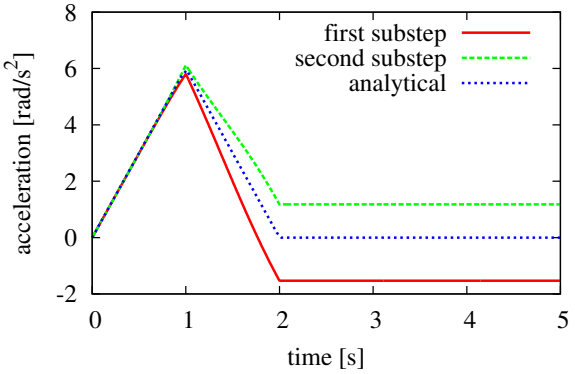

Figure 16: Angular accelerations for $\gamma = 0.85$ vs. time - $\Delta t = 0.01\,s$

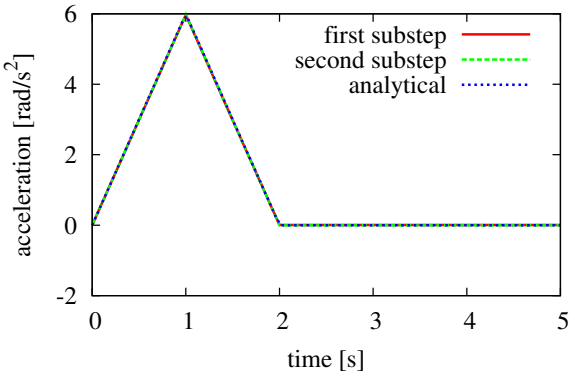

Figure 17: Angular accelerations for $\gamma = 0.731$ vs. time - $\Delta t = 0.01\,s$

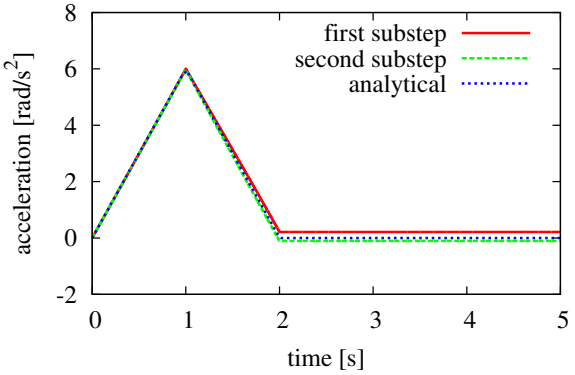

Figure 18: Angular accelerations for $\gamma = 0.5$ vs. time - $\Delta t = 0.001\,s$

4.3 Cantilever beam: Effects of linear and nonlinear behaviour

As a third example a cantilever beam according to [Bathe and Baig(2005)] is investigated. Both linear and a non-linear calculations are performed, where it is focused on the behaviour of the node at the tip of the beam.

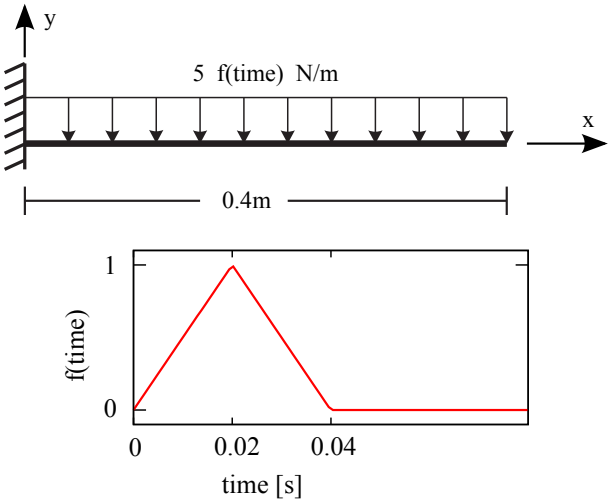

Figure 19: Cantilever beam and loading function f(t)

Fig. 19 shows the system and the associated loading function. A discretization of 20 elements of the previously mentioned two node Timoshenko beam element is used, where it can be chosen between geometrical linear and fully non-linear calculations. The mass allocation is treated by a consistent mass matrix formulation by use of the following model parameters: $E = 70\ 10^9\ N/m^2$, $G = 35\ 10^9\ N/m^2$, $A = 10^{-5}\ m^2$, $I = 8.33\ 10^{-13}\ m^4$, and $\rho = 2700\ kg/m^3$. At first, a linear calculation is performed and the total energy for different values of γ is observed.

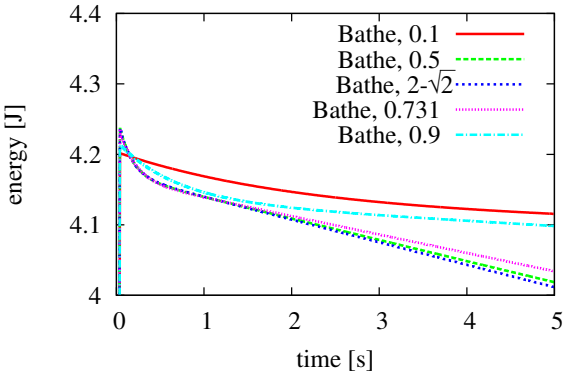

Figure 20: Cantilever beam - Energy dissipation $\Delta t = 0.01$ s - Linear element formulation

Fig. 20 depicts the calculated energy using the scheme with $\Delta t = 0.01\,s$. One can see that the calculated energy is nearly the same when unloading is finished ($t = 0.04\,s$). Regarding the following progression, it can be stated that the scheme exhibits a maximum energy dissipation for $\gamma = 2 - \sqrt{2}$ within the chosen values. The minimum energy dissipation is achieved for $\gamma = 0.1$ and $\gamma = 0.9$. These results are in accordance to Figs. 2 and 4.

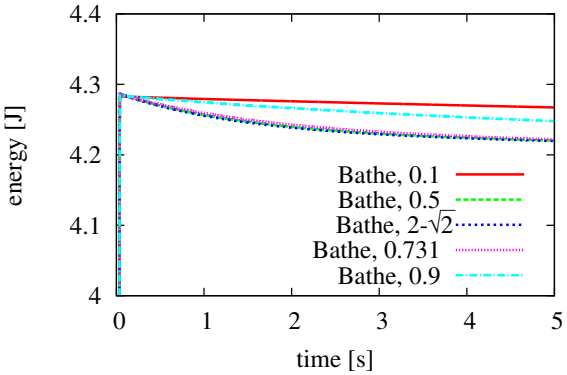

Figure 21: Cantilever beam - Energy dissipation $\Delta t = 0.004$ s - Linear element formulation

Next, the size of Δt is modified to $\Delta t = 0.004\,s$ and the energy dissipation for different values of γ is observed again, cf. Fig. 21. In this case, the curves for $\gamma = 0.5$, $2 - \sqrt{2}$ and 0.731 are almost congruent while the values $\gamma = 0.1$ and 0.9 result in a significant lower energy dissipation. Another point to mention is the overall reduced energy dissipation with the reduced value of Δt. A further reduction of Δt even leads to a further reduce as shown in Figs. 2 and 4.
In the following the same calculations are performed using a non-linear element formulation.

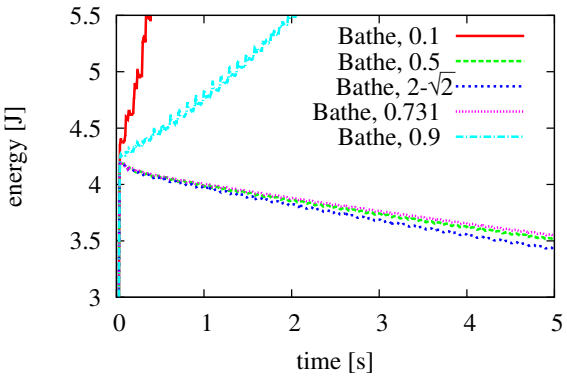

Figure 22: Cantilever beam - Energy dissipation $\Delta t = 0.01\,s$ - Non-linear element formulation

Fig. 22 shows the results for $\Delta t = 0.01\,s$. It can be seen directly that the scheme is no longer stable for any value of γ. While the energy considerably increases for $\gamma = 0.1$ and 0.9 and the scheme gets unstable, the other values of γ still produce stable solutions even though the energy dissipation has drastically increased. Comparing the values of Fig. 20 to Fig. 22, a loss of energy from about $4.25\,J$ to $4\,J$ in the linear case and $4.25\,J$ to $3.5\,J$ in the case of a non-linear calculation can be determined.
In Fig. 23 the results for the reduced time step size $\Delta t = 0.004\,s$ are depicted. Once again the values $\gamma = 0.1$ and 0.9 are unstable. Comparing the results of the remaining values of γ with the ones of the linear calculation, cf. Fig. 21, a higher energy dissipation than in the linear case is observed again.
After having discussed the energy behaviour, the evolution of state variables shall be investigated in more detail. For this purpose, the calculated values in y-direction of the beam are

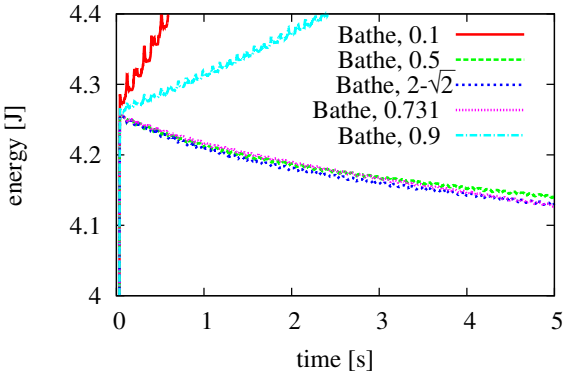

Figure 23: Cantilever beam - Energy dissipation $\Delta t = 0.004\,s$ - Non-linear element formulation

considered, where the analysis is restricted to stable values of γ, based on a time step size of $\Delta t = 0.004\,s$. The calculated displacements and velocities of the model in y-direction using

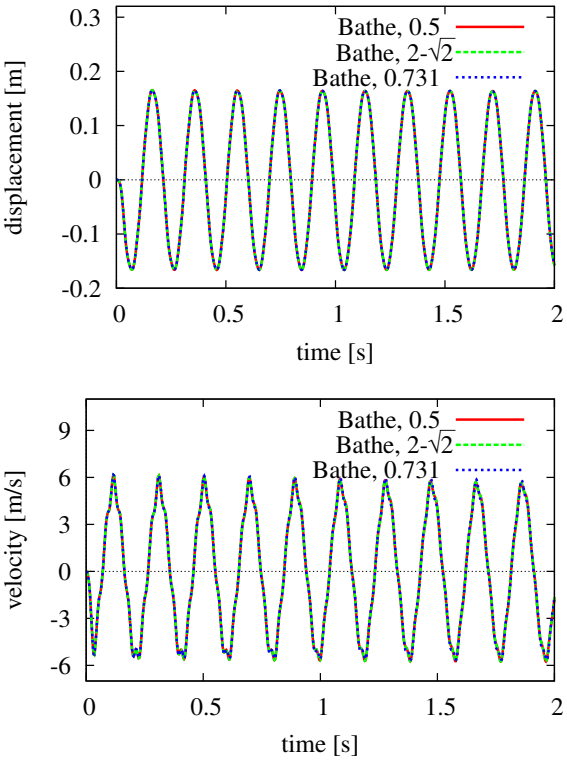

Figure 24: Cantilever beam - Displacement and velocity in y-direction $\Delta t = 0.004$ s - Non-linear element formulation

the non-linear approach are illustrated in Fig. 24. It is clearly visible that all values of γ again lead to almost same results in the plotted time domain.
In Fig. 25 the calculated accelerations in y-direction are presented, when plotting all steps. Slight oscillations at $t \approx 0.04\,s$ with $\gamma = 0.5$ can be observed, while the choice of $\gamma = 0.731$ yields a more smooth solution. However, this effect is marginal and shall be disregarded in the following. On the contrary, the behaviour in x-direction is of higher significance. In order

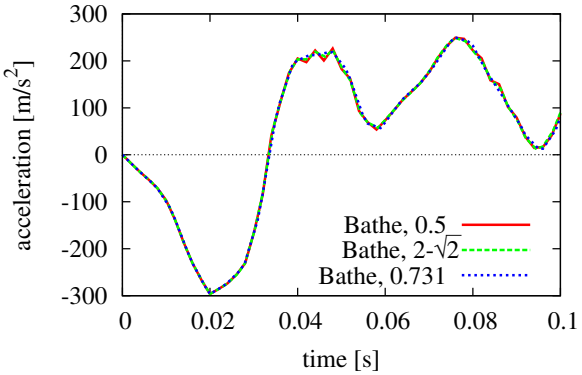

Figure 25: Cantilever beam - Acceleration in y-direction $\Delta t = 0.004\,s$ - Non-linear element formulation

to get more detailed results of the solution, the time step size is reduced to $\Delta t = 0.001\,s$.

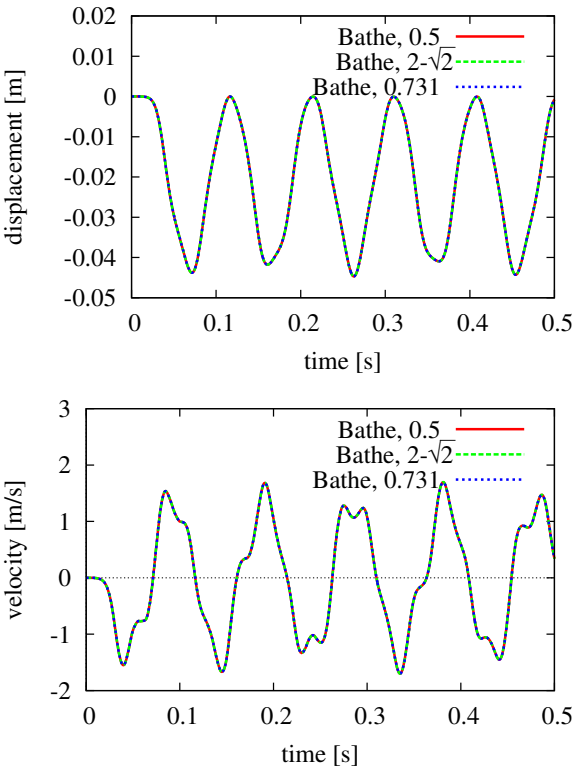

Figure 26: Cantilever beam - Displacement and velocity in x-direction $\Delta t = 0.001$ s - Non-linear element formulation

Fig. 26 shows the calculated displacements and velocities. Again, no visible deviation between the results for different values of γ can be determined.
Fig. 27 depicts the calculated accelerations in x-direction for three different values of γ, each of them illustrated in a separate diagram. As it can be seen, the scheme again produces oscillating accelerations between the first and the second substep. This effect apparently vanishes if a value of $\gamma = 0.731$ is chosen.
In order to make the effect more obvious, the time step size is increased to $\Delta t = 0.004\,s$,

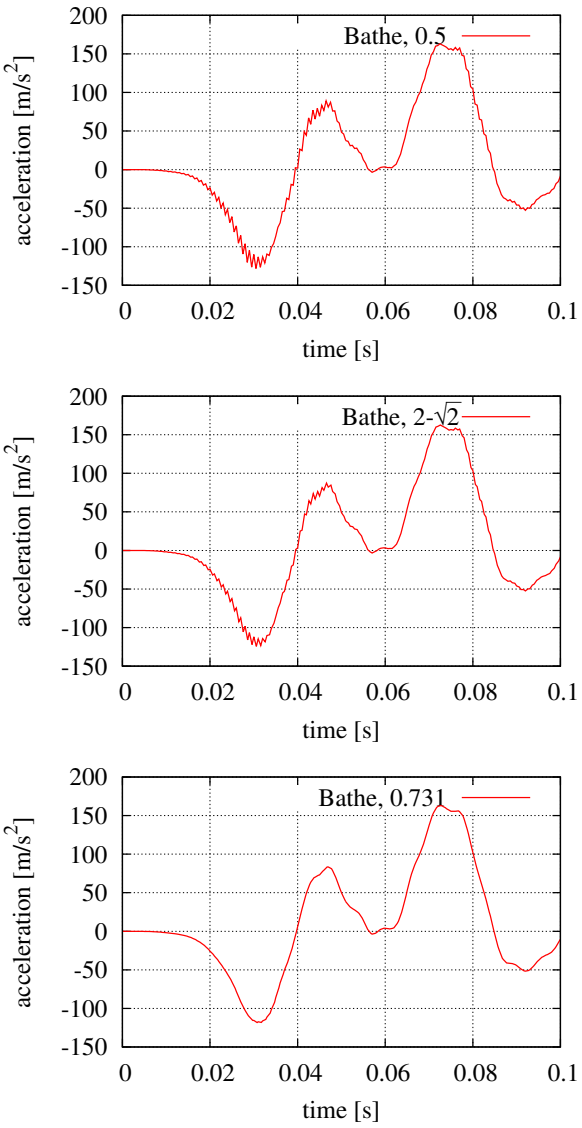

Figure 27: Cantilever beam - Acceleration in x-direction $\Delta t = 0.001$ s - Non-linear element formulation

see Fig. 28. In the first plot three curves are presented connecting points only for the first and the second substep as well as for all available points. It is clear that the first two curves are smooth (but wrong!) while the one, which includes results for the first and the second substep, shows up again oscillations. Comparing these results we can realize, that the first substep solution overshoots the final accelerations while the second one corrects them with too small values. This leads again to the effect that both solutions are partially far away from the correct ones. Considering the second diagram it can be stated that the solution for $\gamma = 0.731$ leads to almost the same results as the one with $\Delta t = 0.001\,s$ without occurring oscillations.

Subsequently, the results of the second substep of the scheme are compared. To this effect Fig. 29 illustrates the solution of the second substep for $\gamma = 0.5$ with $\Delta t = 0.004\,s$ and $\Delta t = 0.001\,s$, as well as the solution for $\gamma = 0.731$ with $\Delta t = 0.004\,s$. It can be seen that the results of the scheme with $\gamma = 0.731/\Delta t = 0.004\,s$ are in good accordance to the results of

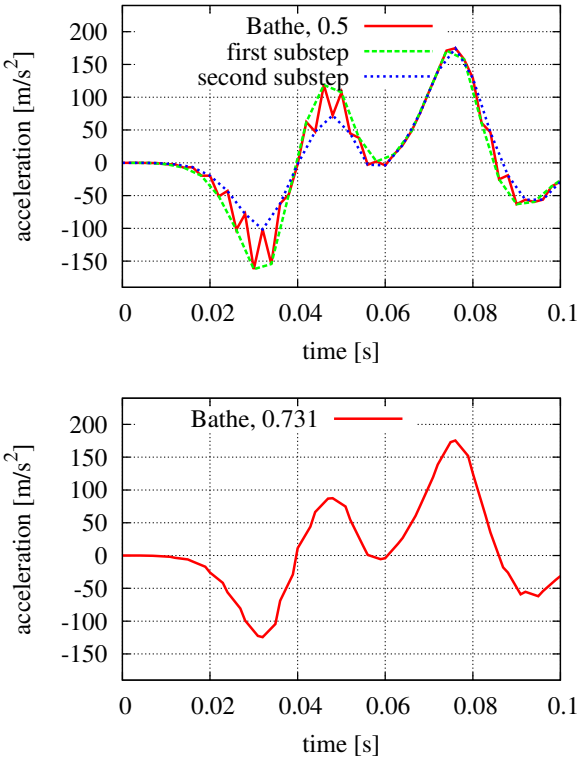

Figure 28: Cantilever beam - Acceleration in x-direction $\Delta t = 0.004$ s - Non-linear element formulation

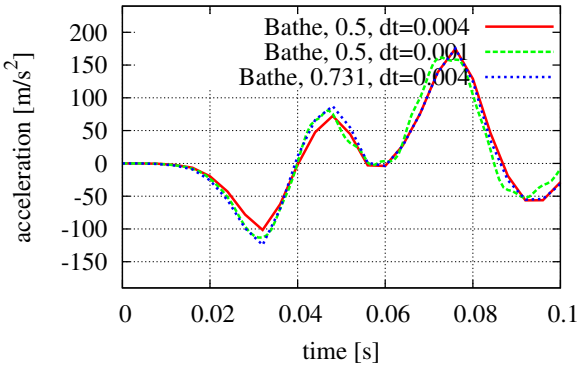

Figure 29: Cantilever beam - Acceleration in x-direction - Comparison results $\gamma = 0.5$ and $\gamma = 0.731$

the scheme with $\gamma = 0.5/\Delta t = 0.001\,s$. Everywhere we observe the oscillating behaviour the results of the scheme with $\gamma = 0.5$ and $\Delta t = 0.004$ s again deviate from the correct solution. While in regions, where no oscillation takes place, the results of $\gamma = 0.5$ and $\gamma = 0.731$ with the same time step size Δt are nearly the same.

Up to now the same element formulation has been used for both examples. In the next step, the Timoshenko beam element will be replaced by a finite rotation Reissner-Mindlin shell element, see [Wagner and Gruttmann(1994)].

The problem is discretized by a mesh of 20×1 four-node elements, while the load is applied normal to the element surface. Further, a lumped mass matrix with row sum technique is

used. The necessary additional data are given by Poisson's ratio $\nu = 0$, thickness $h = 0.001\,m$ and width $b = 0.01\,m$.

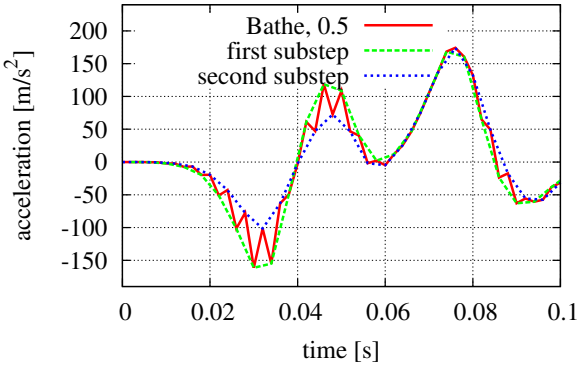

Figure 30: Cantilever beam - Acceleration in x-direction $\Delta t = 0.004$ s - Non-linear shell formulation

Fig. 30 depicts the calculated acceleration in x-direction. Once again, an oscillating behaviour for $\gamma = 0.5$ can be observed, whereas a smooth solution results for $\gamma = 0.731$, as presented for the beam model, see Fig. 28. If both curves are plotted in one diagram hardly any deviation between beam and shell solution can be observed.
By means of this example, it could be shown that the properties of the scheme, regarding numerical damping and stability, change when it is applied to a non-linear instead of a linear calculation. For the linear case, the scheme exhibits numerical damping and unconditional stability for all values of γ, as demonstrated in section 3. In contrast, applying the scheme to non-linear problems, the solution can show an unstable behaviour depending on the chosen value of γ. Concerning the energy plots, there must exist two values of γ for which the scheme is energy conserving. In comparison with the previous model, it is clear, that these value depends at least on the model. Nevertheless, the use of the presented value of $\gamma = 0.731$ apparently suppresses the oscillating acceleration behaviour and leads to accurate solutions in the linear and nonlinear case.

4.4 Propfan

To test the scheme on a larger example, the model of a propfan is chosen, based on artificial data in a preconstruction state [Wagner(1994)].

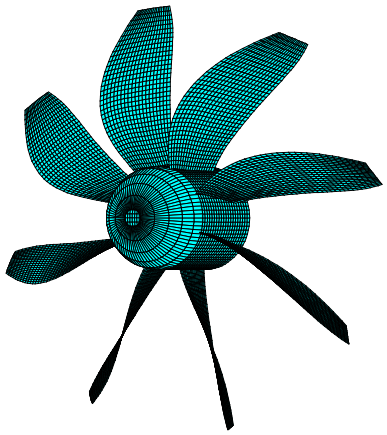

Figure 31: Full model of the propfan

Fig. 31 presents an animation of the full model of the propfan. Based on symmetry conditions the structure can be reduced to a model consisting of only one blade discretized with 802 nodes and 740 shell elements, cf. [Wagner and Gruttmann(1994)].

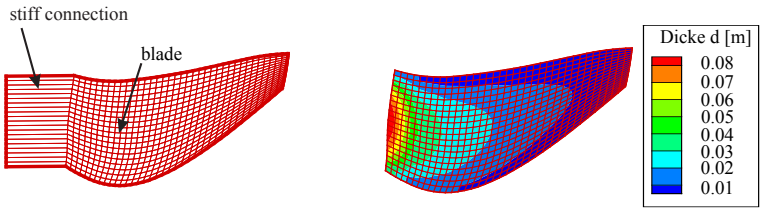

Figure 32: Reduced model of the propfan and thickness distribution

The simplified model and the distribution of the thickness over the blade is depicted in Fig. 32. The stiff part on the left side is introduced to simulate the almost rigid connection of the blade to the rotation axis.

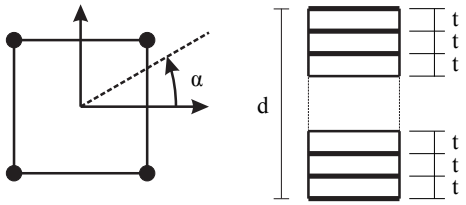

Figure 33: Structure of the blade

The structural setting of the blade in thickness direction consists of six layers with a respective thickness of $t = 0.8\,mm$ and a lay-up $[90, 45, 0, 0, 45, 90]$, see Fig. 33. The associated material parameters of the used transversal isotropic composite material are $E_1 = 135000\,kN/cm^2$, $E_2 = 1000\,kN/cm^2$, $G_{12} = G_{23} = 540\,kN/cm^2$ $\nu_{12} = 0.3$ and $\rho = 1600\,kg/m^3$.
To initiate the rotation of the propfan, we load the structure with a momentum applied on the rotation axis $M(t) = M_0 \cdot f(t)$ with a loading function analogous to Fig. 10 and a value

of $M_0 = 10\,Nm$. Due to the high stiffness and low mass density of the whole model, it is possible to compare the numerical results with the analytical solution for a rigid body motion. For the upcoming investigation the mass moment of inertia is needed

$$\theta = \int r^2 dm \tag{15}$$

It is calculated numerically by use of the discretized finite element model based on the following equation

$$\theta_{FE} = \bigcup_{e=1}^{ne} \sum_{I=1}^{nel} \sum_{K=1}^{nel} \int_{\Omega_e} \int_z (x^2 + y^2) \rho N_I N_K t(z) dz\, dA \tag{16}$$

leading to a value of $\theta = 2.826\ kg \cdot m^2$.
Next, the analytical solution, defined as reference solution, is compared to numerical results gained by different time integration schemes. Hence, with the help of the following diagrams the behaviour of the rotational degree of freedom of the rotation axis is illustrated.
Fig. 34 shows the results determined by means of the trapezoidal rule [Newmark(1959)] in comparison with the analytical solution. Hardly any differences occur concerning the displacements and velocities in the given time range, which confirm the assumption of a almost rigid structure. Nevertheless, one can see that the accelerations already start to oscillate after a few time steps and the scheme becomes unstable.
Fig. 35 presents the results of two time integration schemes using numerical damping, and one energy conserving scheme to achieve stable computations. The first two are the Generalized-α [Chung and Hulbert(1993)] and HHT-α [Hilber,Hughes,Taylor(1977)] scheme, with parameters leading to a spectral radius of $\rho_\infty = 0.8$ for each scheme. The third scheme is the Energy-Momentum-Method [Lewis and Simo(1994)]. Basically, a perfect match between the analytical solution in displacements and velocities is obtained, while there are some oscillations concerning the shape of the accelerations.
Results based on the composite time integration scheme with $\Delta t = 0.01\,s$ are depicted in Fig. 36. The figure shows again a high accordance between the analytical and numerical solutions for displacements and velocities. The accelerations calculated with the values $\gamma = 0.5$ and $\gamma = 2 - \sqrt{2}$ are drawn separately for each substep with dots in the diagram, leading to two separated lines. The results which concern the first substep lie above, the ones concerning the second substep lie below the analytical solution, which simply equals zero for $t > 2s$. Consequently, both curves are not accurate. An oscillation of the accelerations could be depicted by combining the results of the first and second substep. As in the previous examples it can be seen that choosing a value $\gamma = 0.731$ leads to an adequate solution without any oscillations.
In order to emphasize these effects and to get a better insight in the behaviour of the composite scheme, the time step is increased to $\Delta t = 0.05\,s$. The associated results are presented in Fig. 37. Once again, consistent results in comparison to the analytical solution for displacements and velocities are obtained.
On the basis of the larger value of Δt the oscillatory behaviour of the accelerations drastically increases. Similar to the previous diagram the values of the first and second substep lie above and below the analytical solution and lead to non-acceptable values. To this effect it should be emphasized again that the correct solution is $\ddot{\varphi} = 0$ for $t > 2\,s$. However, using the

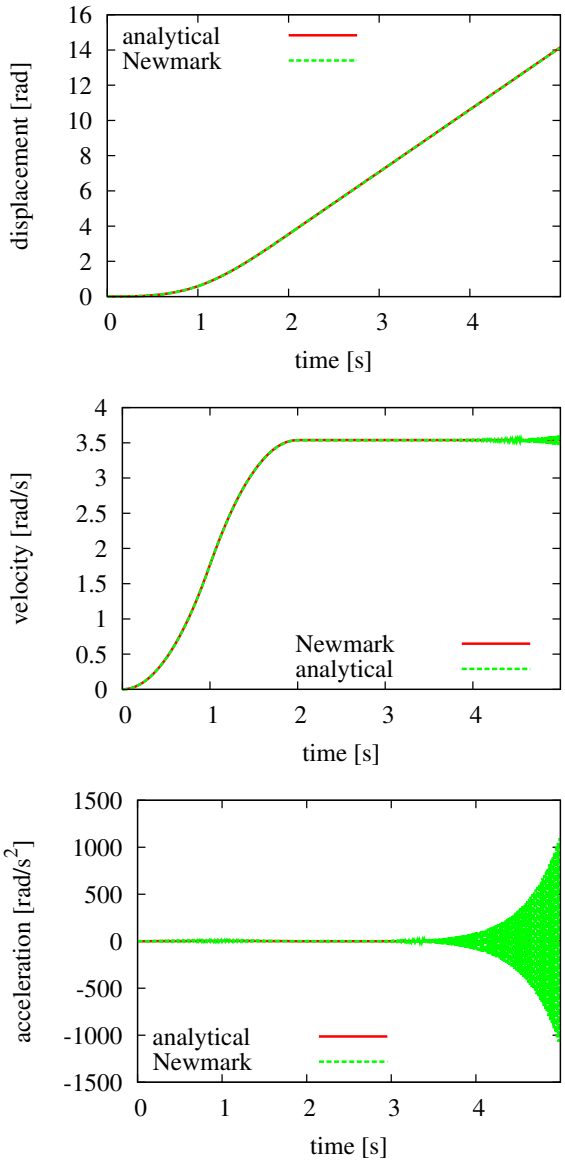

Figure 34: Unstable results with trapezoidal rule - $\Delta t = 0.01$ s

recommended value of $\gamma = 0.731$ still leads to considerably improved results concerning all state variables.

Finally, Fig. 38 illustrates the position of the blade at different time steps during rotation. Regarding the distances between single positions one can clearly ascertain the increasing acceleration of the blade in the range from $t = 0.0\,s$ to $t = 2.0\,s$.

Accordingly, this example demonstrates the fact that the composite scheme is able to produce stable solutions even when applied to a more complex model, provided the value $\gamma = 0.731$ is applied.

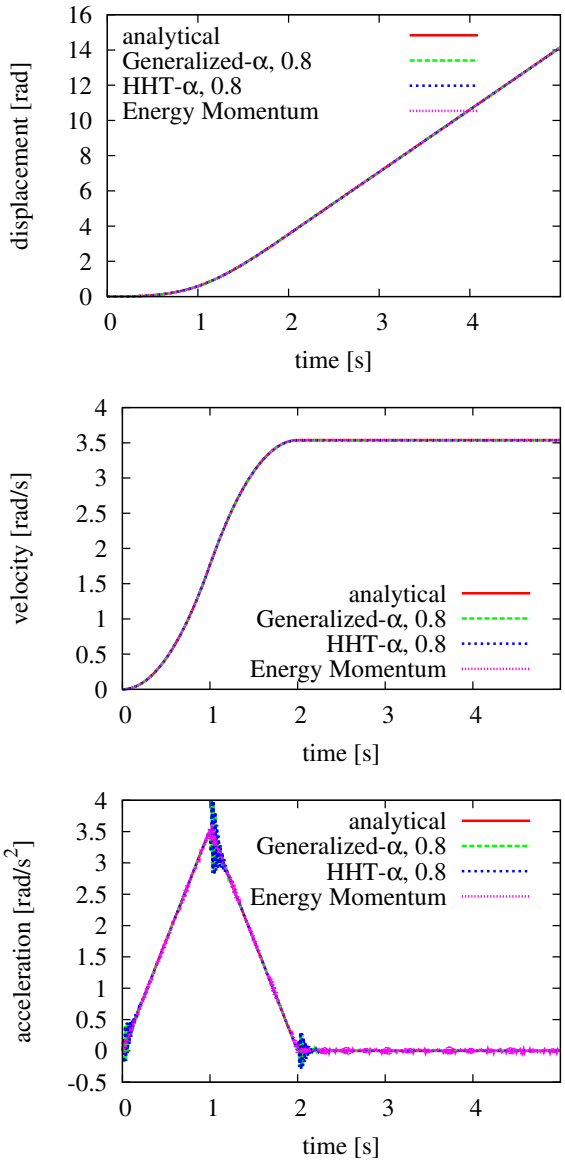

Figure 35: Stable results with different schemes - $\Delta t = 0.01$ s

5 Conclusions

The presented research work is concerned with the application of a common composite time integration scheme proposed by Bathe and co-workers for the investigation of dynamic problems. The simplified extension of the study of the amplification matrix reveals up the fact that the scheme has an 'optimal' value for the free parameter γ in case of linear calculations. Using this value $\gamma = 2 - \sqrt{2}$, the tangent stiffness matrix has to be calculated only once [Bathe and Noh(2012)] and the scheme possesses a minimum of period elongation and maximum numerical damping.

The numerical examples have shown that the scheme loses its properties, i.e. numerical stability independent of γ and numerical damping with respect to γ, when being applied to non-linear problems. Additionally, oscillations occur leading to an incorrect approximation of the accelerations. This effect becomes clearly visible when regarding both, the first and

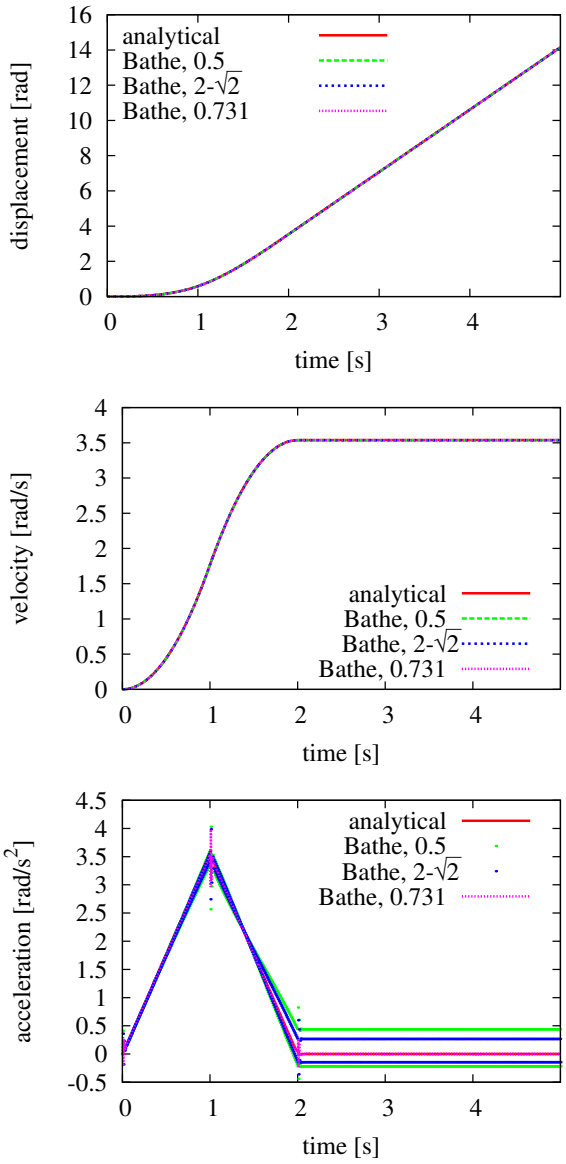

Figure 36: Results of the composite scheme - $\Delta t = 0.01$ s

the second substep, separately. Even if only the second substep is concerned, non-accurate results are obtained. Based on incorrect approximations of the accelerations in the first substep, incorrect approximations are calculated in the second substep as well. To overcome this problem, two options have been tested: the first (classical) one is the choice of a smaller time step size and the second is the application of an 'optimal' value for the parameter γ. On the basis of all performed calculations in the non-linear regime a value of $\gamma = 0.731$ is recommended. As an upcoming task it is highly desirable to find a theoretical and mathematical basis for this result.

Hence, at the present stage the application of the values $\gamma = 2 - \sqrt{2}$ for the linear case and $\gamma = 0.731$ for the geometrically nonlinear case is recommended when applying the presented two-step time integration scheme of Bathe to structural dynamic problems.

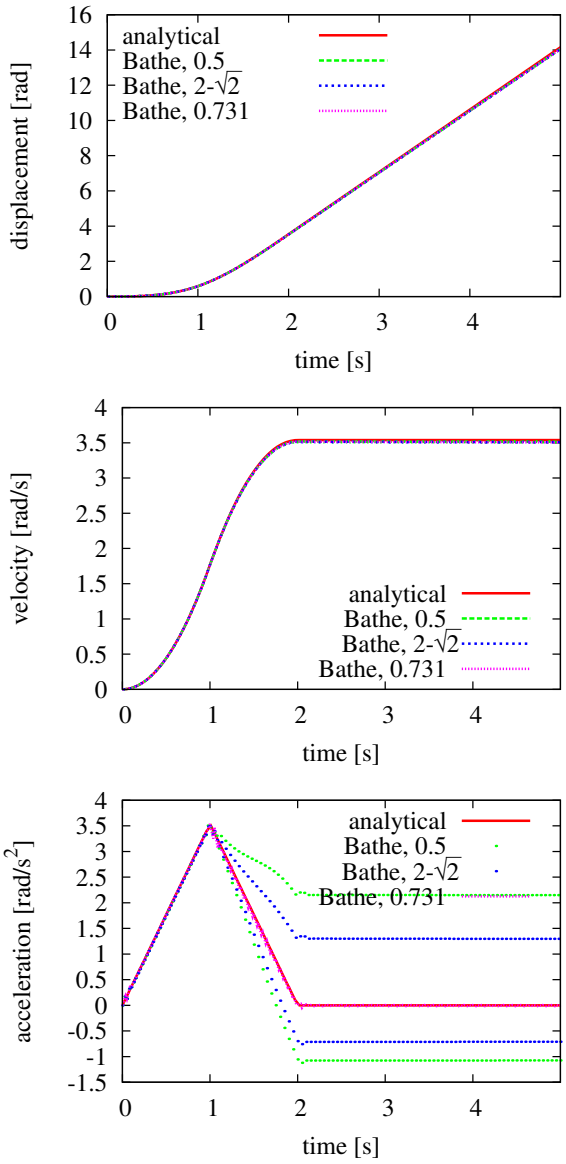

Figure 37: Results of the composite scheme - $\Delta t = 0.05\,s$

References

[Bathe and Baig(2005)] K.-J. Bathe, M. M. I. Baig, On a composite implicit time integration procedure for nonlinear dynamics, Computer & Structures 83 (2005) 2513–2524.

[Bathe(2007)] K.-J. Bathe, Conserving energy and momentum in nonlinear dynamics: A simple implicit time integration scheme, Computer & Structures 85 (2007) 437–445.

[Bathe and Noh(2012)] K.-J. Bathe, G. Noh, Insight into an implicit time integration scheme for structural dynamics, Computer & Structures 98-99 (2012) 1–6.

[Kuhl and Crisfield(1999)] D. Kuhl, M. A. Crisfield, Energy-conserving and decaying algorithms in non-linear structural dynamics, Int. J. Num. Meth. Engng. 45 (1999) 569–599.

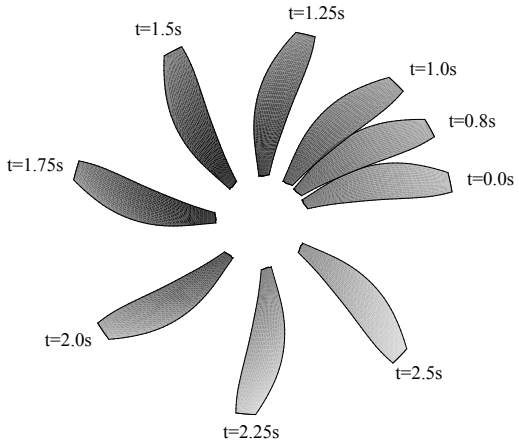

Figure 38: Configuration at different time steps

[Hoff and Pahl(1988)] C. Hoff, P.J. Pahl, Practical performance of the θ_1-method and comparison with other dissipative algorithms in structural dynamics, Computer Meth. in Applied Mechanics and Engineering 67 (1988) 87–110.

[Hoff and Pahl(1988-2)] C. Hoff, P.J. Pahl, Development of an implicit method with numerical dissipation from generalized single step algorithm for structural dynamics, Computer Meth. in Applied Mechanics and Engineering 67 (1988) 367–385.

[Hughes(2000)] T.J.R. Hughes, The Finite Element Method. Linear Static and Dynamic Finite Element Analysis., Dover Publications, New York (2000).

[Newmark(1959)] N. M. Newmark, Newmark A Method of Computation for Structural Dynamics, J. of the Engineering Mechanics Division (1959).

[Matias Silva and Mendes Bezerra(2008)] W. T. Matias Silva, L. Mendes Bezerra, Performance of Composite Implicit Time Integration Scheme for Nonlinear Dynamic Analysis, Mathematical Problems in Engineering 2008 (2008) 1–17.

[Wagner(1990)] W. Wagner, A Finite Element Model for Nonlinear Shells of Revolution with Finite Rotations, Int. J. for numerical methods in engineering (1990) 1455–1471.

[Wagner and Gruttmann(1994)] W. Wagner, F. Gruttmann, A simple finite rotation formulation for composite shell elements, Engineering Computations 11 (1994) 145–176.

[Chung and Hulbert(1993)] J. Chung, G.M. Hulbert, A Time Integration Algorithm for Structural Dynamics With Improved Numerical Dissipation: The Generalized-Alpha Method, J. of Applied Mechanics 60 (1993) 371–375.

[Hilber,Hughes,Taylor(1977)] H.M. Hilber, T.J.R. Hughes, R.L. Taylor, Improved Numerical Dissipation for Time Integration Algorithms in Structural Dynamics, Earthquake Engineering and Structural Dynamics 5 (1977) 283–292.

[Lewis and Simo(1994)] D.I. Lewis, J.C. Simo, Conserving Algorithms for the Dynamics of Hamiltonian Systems on Lie Groups, J. of Nonlinear Science 4 (1994) 253–299.

[Wagner(1994)] W. Wagner, Private Communication with R. Lammering, HSU Hamburg.